

Multi-epoch parsec-scale observations of the blazar PKS 1510-089

M. Orienti^{1,2*}, T. Venturi², D. Dallacasa^{1,2}, F. D’Ammando³, M. Giroletti²,
G. Giovannini^{1,2}, S. Vercellone³, M. Tavani^{4,5}

¹*Dipartimento di Astronomia, Università di Bologna, via Ranzani 1, I-40127, Bologna, Italy*

²*INAF – Istituto di Radioastronomia, via Gobetti 101, I-40129, Bologna, Italy*

³*INAF – Istituto di Astrofisica Spaziale e Fisica Cosmica, via U. La Malfa 153, I-90146 Palermo, Italy*

⁴*Dipartimento di Fisica, Università di Roma “Tor Vergata”, Via della Ricerca Scientifica 1, I-00133 Roma, Italy*

⁵*INAF – Istituto di Astrofisica Spaziale e Fisica Cosmica, via Fosso del Cavaliere 100, I-00133 Roma, Italy*

Received 30 August 2018; accepted ?

ABSTRACT

We investigate the flux density variability and changes in the parsec-scale radio structure of the flat spectrum radio quasar PKS 1510-089. This source was target of multi-epoch Very Long Baseline Interferometer (VLBI) and Space-VLBI observations at 4.8, 8.4 and 22 GHz carried out between 1999 and 2001. The comparison of the parsec-scale structure observed at different epochs shows the presence of a non-stationary jet feature moving with a superluminal apparent velocity of $16.2c \pm 0.7c$. Over three epochs at 8.4 GHz during this period the core flux density varies of about 50%, while the scatter in the jet flux density is within 10%. The polarization percentage of both core and jet components significantly change from 2 to 9 per cent, while the polarization angle of the core shows an abrupt change of about 90 degrees becoming roughly perpendicular to the jet direction, consistent with a change in the opacity. To complete the picture of the physical processes at work, we complemented our observations with multi-epoch Very Long Baseline Array (VLBA) data at 15 GHz from the MOJAVE programme spanning a time baseline from 1995 to 2010. Since 1995 jet components are ejected roughly once per year with the same position angle and an apparent speed between $15c$ and $20c$, indicating that no jet precession is taking place on a timescale longer than a decade in our frame. The variability of the total intensity flux density together with variations in the polarization properties may be explained assuming either a change between the optically-thick and -thin regimes produced by a shock that varies the opacity, or a highly ordered magnetic field produced by the compression of the relativistic plasma by a shock propagating along the jet. Taking into account the high γ -ray emission observed from this source by the AGILE and *Fermi* satellites we investigated the connection between the radio and γ -ray activity during 2007-2010. Multi-wavelength flux and polarization observations suggest that during some γ -ray flaring episodes the emission at high (γ -ray) and low (radio) energies has origin in the same region.

Key words: polarization - galaxies quasars: individual (PKS 1510-089) - radio continuum: general - radiation mechanisms: non-thermal

1 INTRODUCTION

Powerful radio emission is rare in the population of active galactic nuclei (AGN). This phenomenon, only found in about 10% of the AGNs, is associated with the presence of relativistic particles produced in the central regions of the AGN, and then channelled through the jets out to distances

of hundreds of kpc up to a few Mpc. Such relativistic particles are responsible for the synchrotron radiation at the origin of the radio emission. Furthermore, they may scatter low energy photons to high energy bands by inverse Compton (IC) processes, suggesting a connection between radio and high energy γ -ray emission. Indeed, all the γ -ray AGN detected by EGRET are radio-loud sources, strongly supporting this scenario. No radio-quiet AGNs were firmly detected in γ -rays by the Large Area Telescope (LAT) on

* E-mail: orienti@ira.inaf.it

board the *Fermi* satellite during the first year of operation, although possible association for the LAT sources with radio-quiet AGNs are tentatively proposed in the first LAT AGN Catalog (Abdo et al. 2010a). As *Fermi*-LAT continues to collect data and its sensitivity increases, some of these associations could be confirmed.

The AGN dominating the γ -ray sky is the blazar population, comprising flat spectrum radio quasars (FSRQ) and BL Lac objects. These sources are characterized by the presence of a compact radio core, apparent superluminal jet speed, extreme flux density variability in all bands, and high fraction of polarized optical and radio emission. Their observational properties are interpreted as the result of severe beaming effects due to the orientation of the relativistic jet at very small angles to the line of sight.

Thanks to the episodes of enhanced luminosity across the entire electromagnetic spectrum, it is possible to set constraints on the physical properties of the region along the jet responsible for the emission at the various wavelengths. Radio monitoring of EGRET sources suggested that the highest levels of γ -ray emission is observed close in time to radio flares (e.g. Lähteenmäki & Valtaoja 2003), and connected with the emission of a new jet component (Jorstad et al. 2001). Both pieces of evidence give support to the idea that the strongest γ -ray emission is strictly related to a shock in the jet that produces the synchrotron radio flare (e.g. Marscher & Gear 1985). It must be noted that the EGRET data were sparse, with large uncertainties and selection effects, precluding a clear temporal correlation between γ -ray activity and the emission at lower frequencies. The advent of the AGILE and *Fermi* γ -ray satellites allowed us to test the results obtained in the EGRET era, providing details on the connection between γ -ray and radio emission to find out the mechanisms responsible for the high-energy emission. Correlation studies of the first three months of *Fermi*-LAT data and quasi-simultaneous Very Long Baseline Interferometry (VLBI) observations showed that the gamma-ray emitting blazars have faster apparent jet speeds (Lister et al. 2009a), wider apparent opening angles (Pushkarev et al. 2009), and higher variability and Doppler factor (Savolainen et al. 2010), with respect to blazars with weak γ -ray emission. Variability studies from radio to high energy bands give important insight to locate the site of flares and infer the physical conditions of the jet. In particular, using the most recent γ -ray as well as radio polarimetric data, a likely close connection between high γ -ray states and the activity in the pc-scale core region has been investigated (see e.g. Agudo et al. 2011). In addition, Pushkarev et al. (2010) found for a sample of 186 sources a non-zero time delay between radio emission measured by pc-scale observations at 15 GHz and γ -ray radiation detected by *Fermi*-LAT, suggesting that the delay is most likely connected with synchrotron opacity in the core region.

Among blazars, PKS 1510-089 is an ideal target to investigate the location of the emitting region and the physical processes occurring in relativistic jets. This object is a flat spectrum radio quasar at $z = 0.361$ (Thompson et al. 1990) with highly polarized optical emission. The synchrotron emission has its peak in the IR band, while the inverse Compton component peaks in the γ -ray regime. High flux density variability is observed throughout the

electromagnetic spectrum, from the radio to the high energy bands. In particular, episodes of high γ -ray activity were recently detected by both *Fermi*-LAT (Cutini & Hays 2009; Ciprini & Corbel 2009; Tramacere 2008) and the Gamma Ray Imaging Detector (GRID) on board AGILE (Striani et al. 2010; Vercellone et al. 2009; Pucella et al. 2009; D’Ammando et al. 2009a, 2008). Description of these events, together with their possible connection with multiwavelengths emission can be found in Pucella et al. (2008), D’Ammando et al. (2009b), Marscher et al. (2010), Abdo et al. (2010b), and D’Ammando et al. (2011).

In the radio band the emission is dominated by the core component. Multi-epoch parsec-scale observations revealed highly superluminal knots with apparent velocity exceeding $20c$ (e.g. Homan et al. 2001; Jorstad et al. 2005; Lister et al. 2009b; Marscher et al. 2010), ejected along the north-west direction at an angle of about -30° with respect to the core. On arcsecond scale the jet structure is oriented in the opposite direction, indicating a severe misalignment of almost 180° between the pc- and kpc-scale jet. Misalignment between pc- and kpc-scale structure has been frequently observed in core-dominated sources (e.g. Pearson & Readhead 1988). However, misalignment larger than 110° as those found in 0954+556 and 1652+398 (Lister et al. 2001) is very rare. The extraordinary case of PKS 1510-089 has been described by Homan et al. (2002a) assuming a small change of about 12° - 24° in the intrinsic jet direction, that appears amplified due to projection effects, providing a simple explanation for the observed morphology. Both the misalignment and the highly superluminal jet speed indicate that the jet axis of PKS 1510-089 forms a very small angle of a few degrees to the line of sight. Such an extreme orientation enhances beaming effects making this source a good target to investigate the possible connection between γ -ray flares and the ejection of jet components.

In this paper we present new results of proprietary multi-epoch polarimetric VLBI and Space-VLBI observations of PKS 1510-089 carried out at 4.8, 8.4 and 22 GHz between 1999 and 2001 and not yet published, with the aim of studying changes in the source structure and investigating their possible connection with other physical properties, such as flux density variability, spectral index distribution and polarization properties. We then compare our results with multi-epoch Very long Baseline Array (VLBA) data at 15 GHz from the MOJAVE (Monitoring Of Jets in Active galactic nuclei with VLBA Experiments) programme¹ (Lister et al. 2009c) spanning a larger time interval, between 1995 and 2010. The addition of high energy information from AGILE and *Fermi* data gives us a clue to connect γ -ray emission and radio properties, like flux density variability and changes in the pc-scale radio structure for the period 2007–2010.

Throughout this paper, we assume the following cosmology: $H_0 = 71 \text{ km s}^{-1} \text{ Mpc}^{-1}$, $\Omega_M = 0.27$ and $\Omega_\Lambda = 0.73$, in a flat Universe. At the redshift of the target 1 arcsec =

¹ All the 15-GHz data presented in this paper are from the MOJAVE programme. The MOJAVE data archive is maintained at <http://www.physics.purdue.edu/MOJAVE>.

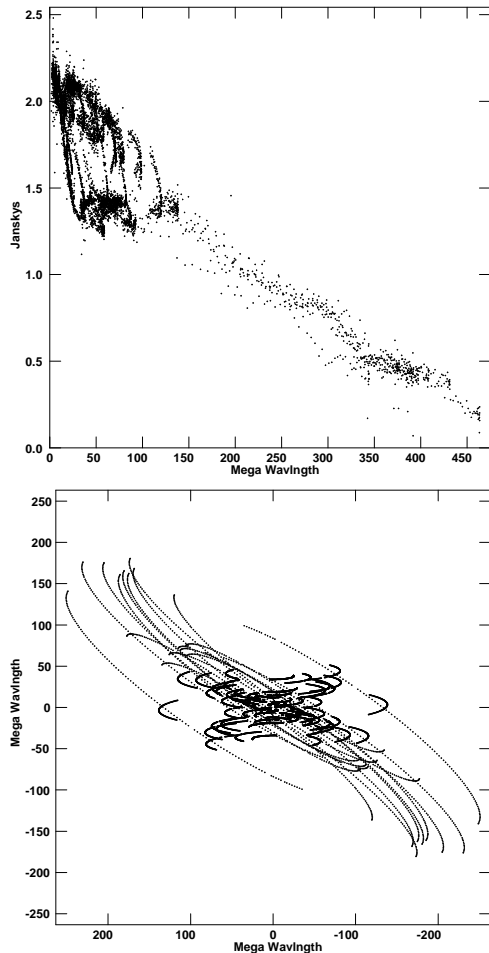


Figure 1. Plot of amplitude vs. projected baseline length at 4.8 GHz (*top*), and the uv coverage (*bottom*) of Space-VLBI (VSOP) observations.

5.007 kpc. The spectral index α is defined as $S(\nu) \propto \nu^{-\alpha}$.

2 RADIO DATA

2.1 VLBI and Space-VLBI observations

PKS 1510-089 was target of Space-VLBI observations. It was observed at 4.8 GHz (C band) by VLBA+HALCA on 1999 August 11 and on 2000 May 13 in single polarization mode. In each observing run the target was observed for about 6 hours. Examples of the uv coverage and amplitude vs. baseline length are presented in Fig. 1.

The target source was observed with the VLBA with the addition of the Effelsberg telescope at 8.4 GHz (X band) and 22.2 GHz (K band), in full polarization mode with a bandwidth of 32 MHz at 128 Mbps. To study possible changes in the source structure, subsequent VLBA observations at 8.4 GHz were carried out in full polarization with a recording bandwidth of 32 MHz at 128 Mbps. The correlation was performed at the VLBA correlator in Socorro and the data reduction was carried out with the NRAO AIPS

package. In the X band the instrumental polarization was removed by using the AIPS task PCAL. The absolute orientation of the electric vector of the calibrator B1749+096 was then compared with the VLA/VLBA polarization calibration database to derive the corrections. The values derived are in good agreement ($\leq 5^\circ$).

Final images for each epoch and at each frequency were produced after a number of phase self-calibration iterations. Amplitude self-calibration was applied at the end of the process using a solution interval longer than the scan length, to remove residual systematic errors and to fine tune the flux density scale, but not to force the individual data points to follow the model. The resolution at the various frequencies are almost comparable (Table 1) due to the similar uv -coverage reached with the different interferometers used. At 8.4 GHz, besides the total intensity (I), images in the Stokes' U and Q parameters were produced with the final fully calibrated datasets. Final VLBI images at 4.8, 8.4 and 22.2 GHz are shown in Fig. 2. For the observations carried out on 1999 January 11, we produced also a low-resolution image at 22.2 GHz using the same uv range, restoring beam and image sampling of the 8.4 GHz data in order to produce the spectral index image, which is presented in Fig. 3 superimposed on the 22.2 GHz contours obtained from the low-resolution image. Information on the VLBI observations is reported in Table 1.

2.2 MOJAVE data

To study the radio variability of PKS 1510-089, we compared our observations with multi-epoch 15-GHz (U band) VLBA data from the MOJAVE programme spanning a time interval from 1995 July 28 to 2010 December 23. The typical resolution is about 1.4×0.5 mas. For each of the 51 epochs analysed, we imported the calibrated uv -datasets (Lister et al. 2009c) into the NRAO AIPS package and performed a few phase-only self-calibration iterations before producing the final total intensity images which resulted to be fully consistent with those reported by Lister et al. (2009c). For those datasets in full polarization mode, we produced also Stokes' U and Q images. The rms noise level measured on the image plane is in the range of 0.15 and 0.3 mJy/beam. Total intensity images concerning the observing epochs between July 1995 and July 2008 are published in Lister et al. (2009c). An image of the source structure in September 2010 is presented in Fig. 4 as an example.

2.3 Data analysis

The flux density and deconvolved angular size of each source component were measured by means of the AIPS task JMFIT, which performs a Gaussian fit to the source components on the image plane. For extended components like the low-surface brightness diffuse jet visible at 8.4 GHz, the flux density was derived by means of TVSTAT, which performs an aperture integration over a selected region on the image plane. When the polarization information was available, we derived the polarization parameters, such as the linearly polarized flux density, the fractional polarization, and the (integrated) position angle of the electric

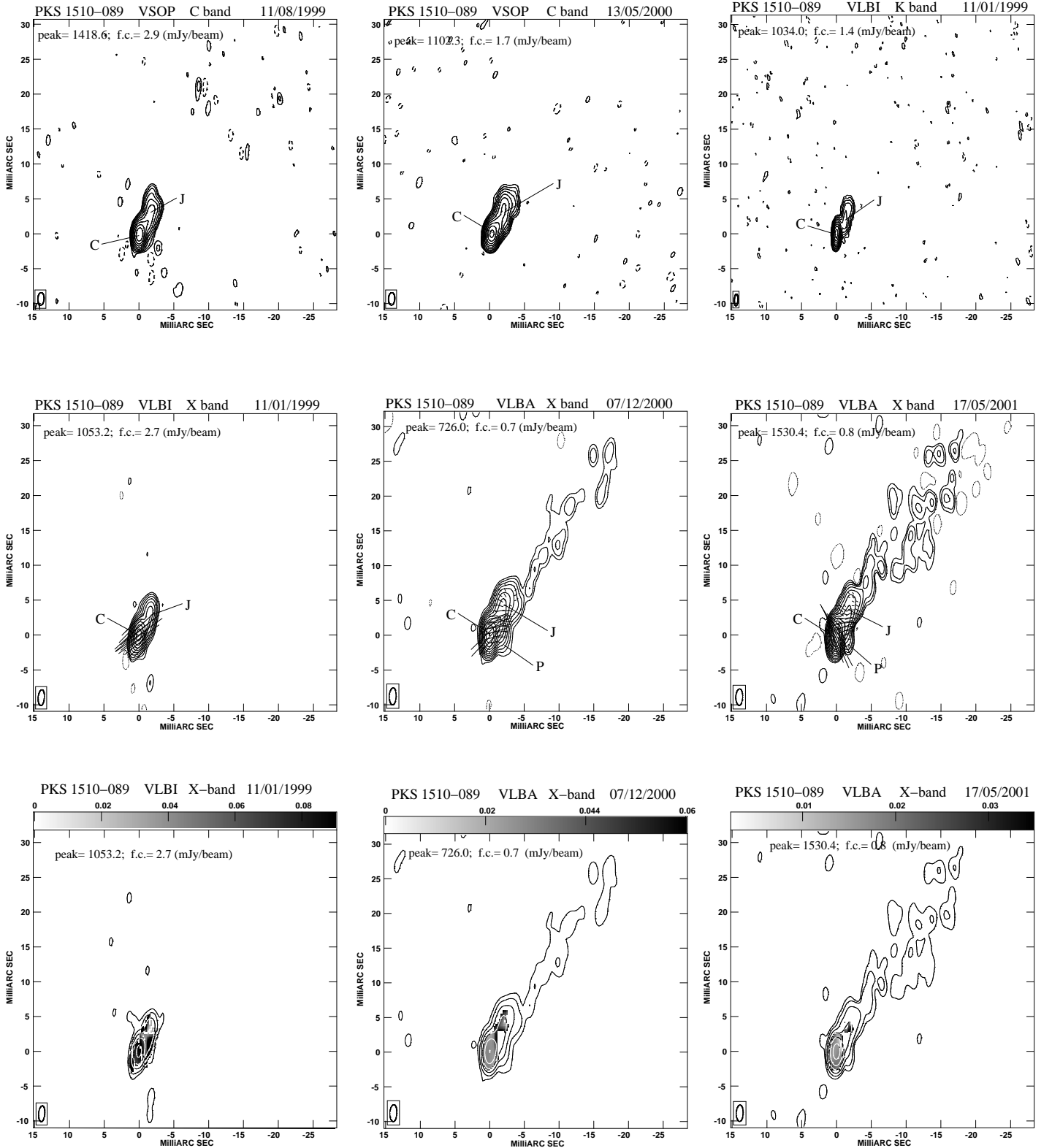


Figure 2. VLBI images of the source PKS 1510-089. *Upper panel:* total intensity VSOP images at 5 GHz and VLBI image at 22 GHz. *Middle panel:* total intensity VLBA images at 8.4 GHz. *Bottom panel:* fractional polarization images at 8.4 GHz. On each image we provide the telescope array, the observing band and the observing date; the peak flux density in mJy/beam and the first contour (f.c.) intensity in mJy/beam, which corresponds to three times the off-source noise level. Contour levels increase by a factor 2 in the upper and middle panels, and a factor 4 in the bottom panel. The restoring beam is plotted on the bottom left corner. For the datasets with polarization information, the vectors superimposed on the I contours show the position angle of the \vec{E} vector, where one-millimeter length corresponds to 2.5 mJy/beam. The greyscale represents the fractional polarization.

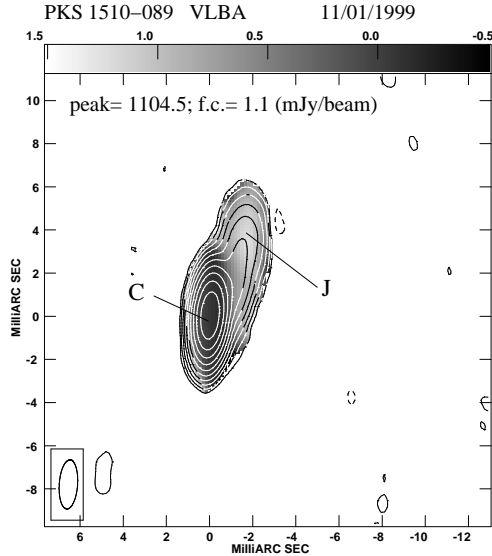


Figure 3. Spectral index distribution between 8.4 and 22.2 GHz across the target source PKS 1510-089 superimposed on the 22.2 GHz contours convolved to the 8.4-GHz beam. On the image we provide the peak flux density in mJy/beam and the first contour (f.c.) intensity in mJy/beam corresponding to three times the off-source noise (1σ). Contour levels increase by a factor 2. The restoring beam is plotted on the bottom left corner.

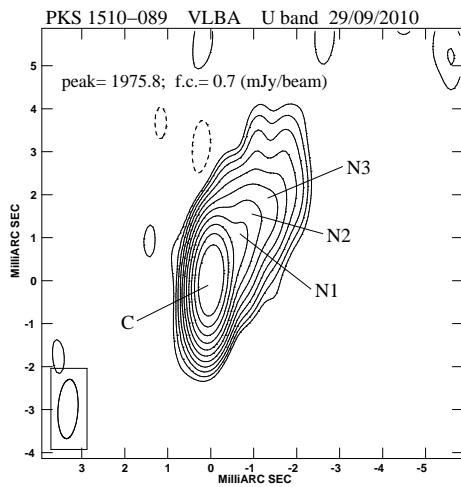


Figure 4. An example of the VLBA image at 15 GHz relative to 2010 September 29. On the image we provide the observing band, the peak flux density in mJy/beam and the first contour (f.c.) intensity in mJy/beam, which corresponds to three times the off-source noise level. Contour levels increase by a factor 2. The restoring beam is plotted on the bottom left corner.

vector \vec{E} . In Table 2 we report the source parameters concerning our proprietary observations at 4.8, 8.4, 22 GHz and listed in Table 1.

In addition to the data analysis performed on the image plane, a further modelfitting with Gaussian components was carried out to the visibility data at each epoch using the modelfitting option in Difmap. This approach is preferable

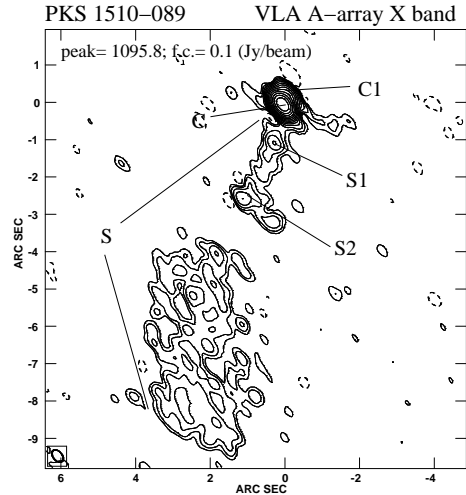


Figure 5. VLA A-array image at 8.4 GHz of PKS 1510-089 produced from archival data (project AF376) and calibrated using the standard procedure developed in the NRAO AIPS package. On the image we provide the observing band, the peak flux density in mJy/beam and the first contour (f.c.) intensity in mJy/beam, which corresponds to three times the off-source noise level. Contour levels increase by a factor 2. The restoring beam is plotted on the bottom left corner.

in the case we want to derive small variations in the source structure. Indeed, the analysis of the visibility data allows us to use the full resolution capability of the interferometer, without the dependence of the beam and sampling used in producing the image. Furthermore, it provides more accurate fit of unresolved structures close to the core component, as the case of new jet features, thus yielding to a better determination of the position of each component.

3 RESULTS

3.1 Morphology

The radio emission of PKS 1510-089 is dominated by the bright core component from which a pc-scale jet emerges at an angle of about -30° (Fig. 2). The pc-scale jet is not straight, but it bends at about 2 mas (10 pc) from the core, and its emission progressively fades until 5 mas (25 pc) where it goes below the detection limit, in agreement with images at other frequencies (e.g. Homan et al. 2002a; Jorstad et al. 2005; Lister et al. 2009c). Furthermore, an additional component almost perpendicular to the jet axis, visible in several observing epochs and labelled P in Fig. 2, is present at about 2 mas West from the core. This component is present only in the 15-GHz images with the highest signal-to-noise level precluding a reliable discussion on its nature.

In our deep VLBA observations at 8.4 GHz (Fig. 2) a low-surface brightness diffuse jet is visible up to about 25 mas (125 pc) from the core.

From the spectral index image (Fig. 3) produced comparing the simultaneous observations at 8.4 and 22.2 GHz we find

Table 1. VLBI observations of PKS 1510-089.

Freq GHz	Code	Obs. date	Dur. h	rms mJy/b	Beam mas×mas	Array
4.8	W004	1999 Aug 11	6	0.97	1.80×0.90	VLBA+HALCA
4.8	W004	2000 May 13	6	0.57	1.80×0.90	VLBA+HALCA
8.4	BV027	1999 Jan 11	1	0.90	2.29×0.88	VLBA+EF
8.4	BV042	2000 Dec 7	1.5	0.23	2.44×1.00	VLBA
8.4	BV042	2001 May 17	1.5	0.27	2.36×0.99	VLBA
22.2	BV027	1999 Jan 11	1.5	0.47	1.70×0.49	VLBA+EF

Table 2. VLBI observational parameters of PKS 1510-089 for the observing epochs reported in Table 1.

Comp	ν_{obs} GHz	S_{ep1} mJy	S_{ep2} mJy	S_{ep3} mJy	Pol _{ep1} mJy (%)	Pol _{ep2} mJy (%)	Pol _{ep3} mJy (%)	χ_{ep1} deg	χ_{ep2} deg	χ_{ep3} deg
C	4.8	1504	1161	-	-	-	-	-	-	-
C	8.4	1120	807	1560	98 (8.6%)	23 (2.8%)	26 (1.6%)	140	110	16
C	22.2	1139	-	-	-	-	-	-	-	-
J	4.8	626	644	-	-	-	-	-	-	-
J	8.4	236	261	244	15 (6.3%)	13 (5.0%)	7 (2.9%)	70	77	100
J	22.2	143	-	-	-	-	-	-	-	-
Diffuse J	8.4	-	34	70	-	-	-	-	-	-

that the core component has a slightly inverted spectrum ($\alpha = -0.02$), while in the jet the spectral index is 0.5 close to the core and steepens moving outwards.

This initial part of the jet ($0.3''$, i.e. 1.5 kpc) is also visible in the VLA image at 8.4 GHz (Fig. 5) as the “northern component” C1, in the opposite direction of the kpc-scale structure (labelled S). The large scale structure is roughly collimated up to a distance of about 2 arcsecond (10 kpc) from the core. Then it slightly bends to the West, forming an extended low-surface brightness lobe-like feature. Two compact regions (S1 and S2 in Fig. 5), likely jet knots, are located at $1.0''$ (~ 5 kpc) and $2.7''$ (~ 13 kpc) from the core.

3.2 Flux density and polarization

The analysis of the radio lightcurves of PKS 1510-089 shows strong flux density variability, where low states alternate with flares (Venturi et al. 2001; Jorstad et al. 2001; Hughes et al. 1992). Sometimes additional episodes of abrupt flux density increase have been registered. These studies are based on single-dish observations where it is not possible to disentangle the contribution of the jet from the one arising from the core, and changes in the parsec-scale structure may be washed out by the contribution of the stationary components. The availability of high-resolution VLBI data allows us to separate the core and jet emission and thus to determine how the flux density changes in both components. Comparing our three-epoch data at 8.4 GHz (Table 1) we find that the core flux density varies of

about 50% between 1999 and 2001, while the scatter in the jet flux density is within 10%. We compare the flux density lightcurve at 8.4 GHz with the 15-GHz VLBA data from the MOJAVE programme (Lister et al. 2009c) obtained between 1998 and 2001. In Figs. 6a,b we report the flux density of the core and jet components. The core flux density at 15 GHz clearly shows strong variability reaching a maximum in October 1999, when it has almost doubled its value, then followed by a clear decrease lasting till the end of 2001 (Fig. 6a). After this period the core flux density increases again, in agreement with the trend found at 8.4 GHz, but the observations are quite sparse precluding a more detailed study of the core variability. On the other hand, the jet flux density at 15 GHz varies about 25% till the end of 2000, while the scatter increases in 2001 (Fig. 6b). The jet flux density has more moderate variability than the core. Despite the lack of simultaneous multifrequency observations, we can confirm a steep overall spectral index for the jet ($\alpha = 0.5 - 0.7$) between 8.4 and 15 GHz. On the other hand a characteristic value of the spectral index of the core could not be determined due to its strong and irregular variability associated with changes in the opacity. A realistic value for the core spectral index could be derived only for the observations carried out on January 1999 when simultaneous observations at 8.4 and 22 GHz are available, providing a flat spectral index (Fig. 3).

The polarization properties of both core (Fig. 6c,e) and jet (Fig. 6d,f) components are quite different. In the three observing epochs at 8.4 GHz we find that both the core

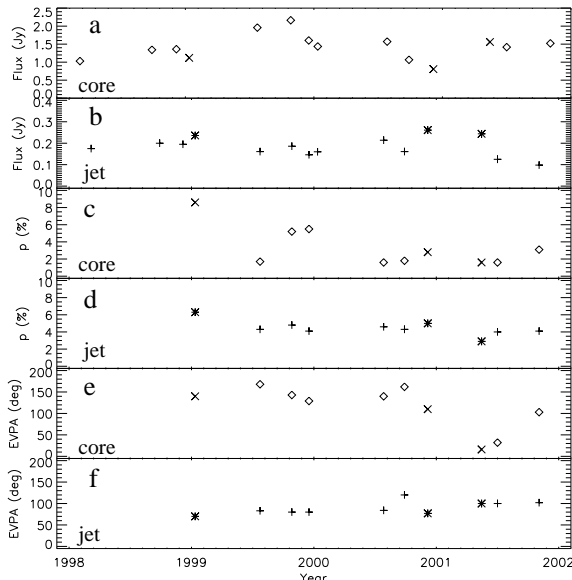


Figure 6. Total intensity and polarization properties at 8.4 and 15 GHz of PKS 1510-089. Core parameters are marked by a diamond at 15 GHz, and by a cross at 8.4 GHz. Jet parameters are marked by a plus sign at 15 GHz and by an asterisk at 8.4 GHz. *Panel a:* total intensity flux density of the core; *panel b:* total intensity flux density of the jet; *panel c:* fractional polarization of the core component; *panel d:* fractional polarization of the jet component; *panel e:* position angle of the electric vector (EVPA) of the core component; *panel f:* EVPA of the jet component. Uncertainties are within the symbols.

and the jet are polarized with a fractional polarization varying between 1.6 and 8.6 per cent in the core region, and about 2.9 and 6.3 per cent in the jet (Table 2, bottom panel of Fig. 2, and Fig. 6c,d). At 15 GHz the polarization percentage of the core is very variable, between 1.6 and 5.5 per cent (Fig. 6c), and shows no evident correlation with the total intensity flux density. On the other hand, the polarization percentage of the jet at 15 GHz (Fig. 6d) is roughly constant around 4.5 per cent. In the core component the position angle of the electric vector \vec{E} (EVPA) at 8.4 GHz is 140° and 110° during the first two epochs, then it changes abruptly in May 2001, when it is 16° . A similar behaviour is found at 15 GHz, where the EVPA is between 168 and 130 degrees from 1999 to 2000, i.e. roughly parallel to the jet axis, while in June 2001 it is 32 degrees (Fig. 6e), becoming perpendicular to the jet direction. On the other hand, the jet EVPA does not show such a large variation, being between 80 and 100 degrees, with the exception of September 2000 when it turned out to be 120 degrees. We note that only the integrated rotation measure (RM) is available for this source (-15 ± 1 rad m^{-2} , Simard-Normandin et al. 1984). The corrections to the observed EVPA to obtain the intrinsic orientation are therefore negligible.

3.3 Proper motion

The multi-epoch analysis of the pc-scale morphology of PKS 1510-089 shows a considerable evolution of the source structure: jet components emerge from the core at different times and their changes can be followed by comparing observations carried out after short time intervals. With the aim of characterizing variations in the source structure we modelfitted the visibility data at each epoch (see Section 2.3). Direct comparison of models obtained independently at each epoch is not the best approach to detect small changes (Conway et al. 1992). For this reason, we produced a zero-order model consisting of 3 elliptical Gaussian components, which was used as the initial model in modelfitting the visibility data of each observing epoch. Errors Δr associated with the component position were estimated by means of:

$$\Delta r = a / (S_p / \text{rms}) \quad (1)$$

where a is the component deconvolved major axis, S_p is its peak flux density and rms is the 1σ noise level measured on the image plane (Polatidis & Conway 2003). In the case the errors estimated by Eq. 1 are unreliably small, we assume a more conservative value for Δr that is 10% of the beam. The data points are then fitted by a linear model that minimizes the chi-square error statistic.

The linear fit on the three epochs of 8.4-GHz data (Table 1 and Fig. 2) provides an angular separation rate of 0.990 ± 0.040 mas/yr that corresponds to $\beta_J = 16.2 \pm 0.7$. From the linear back extrapolation fit, and considering the uncertainties on the fit parameters, we estimate the time of zero separation T_0 between the jet component and the core, that results to be $T_{0,J} = 1997.42 \pm 0.12$. The accuracy of the fit has been tested also by comparing the component separation derived by modelfitting the visibility of the two epochs 4.8-GHz Space-VLBI data and the three epochs at 15 GHz available from the MOJAVE project in the same time interval (left panel in Fig. 7), all with a similar resolution.

To extend the analysis of the knot separation speed till the end of 2010, we modelfitted the data at 15 GHz from the MOJAVE programme. Results from the analysis of data between 1995 and 2008 were already published in previous works by Homan et al. (2001) and Lister et al. (2009b), where the separation velocities found for the detected knots range between $15c$ and $20c^2$. Since 2007, when also *Fermi* and *AGILE* satellites could provide crucial information to relate the radio and high-energy γ -ray emission, we could follow the evolution of three additional knots, labelled N1, N2 and N3 in Fig. 4. For N1, a 1σ separation speed of $675 \mu\text{as/yr}$ (i.e. $11.6c$) was reported by Abdo et al. (2010b) using data between September 2008 and December 2009. In our analysis we expand the time baseline to December 2010. We determine the angular separation speeds of these three new knots from the core, which we assume stationary: we derive 1.060 ± 0.056 mas/yr, 1.102 ± 0.113 mas/yr, and 1.041 ± 0.250 mas/yr for N1, N2 and N3 respectively, which correspond to $\beta_{N1} = 17.3 \pm 0.9$, $\beta_{N2} = 18.0 \pm 1.9$, $\beta_{N3} = 17.0 \pm 4.0$.

² In the Appendix, we re-modelfitted these datasets in order to compare results obtained with a consistent approach.

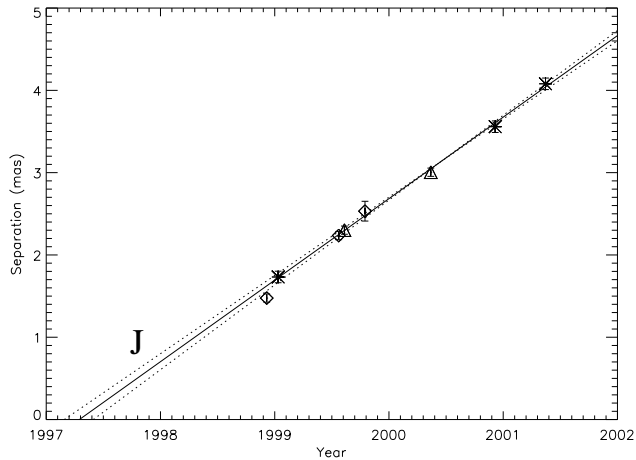


Figure 7. Changes in separation with time between components C and J. Asterisks, diamonds, and triangles refer to 8.4-GHz VLBA data, 15-GHz VLBA data, and 4.8-GHz Space-VLBI (VSOP) data respectively. The solid line represents the regression fit to the 8.4-GHz VLBI data, while the dashed-lines represent the uncertainties from the fit parameters. Error bars are determined as in Section 3.3.

For each knot the time of zero separation obtained from the fit is $T_{0,N1} = 2008.61 \pm 0.11$, $T_{0,N2} = 2009.38 \pm 0.17$, and $T_{0,N3} = 2009.93 \pm 0.25$ (Fig. 8). Components N1 and N2 were also detected in VLBA observations at 43 GHz by Marscher et al. (2010). Given the lower spatial resolution (and larger opacity) with respect to the 43 GHz, these components were detected at 15 GHz a few months later when their separation from the core was large enough to be resolved. The apparent separation speeds derived at 43 GHz are 24 ± 2 and 21.6 ± 0.6 for N1 and N2 respectively, i.e. systematically larger than our values. This discrepancy may be due to the lower resolution of the 15-GHz data that may cause a blending with other features, as also suggested in Abdo et al. (2010b). However, it must be noted that the higher separation speed found at 43 GHz is not reflected in a substantially different origin time of the jet components. In fact, in the case of N1 and N2 components the time of zero separation derived from 43-GHz data are 2008.57 ± 0.05 and 2009.34 ± 0.01 respectively (Marscher et al. 2010), i.e. within the errors estimated from the 15-GHz data. In Table 3 we report the apparent separation speed and the ejection date of the superluminal knots of PKS 1510-089.

4 DISCUSSION

The population of blazar objects represents a sub-class of AGN characterized by high levels of flux density variability across the entire electromagnetic spectrum. In the radio band the increase in luminosity is first detected at high frequencies, at millimeter wavelengths, subsequently followed at lower frequencies with some delay, consistent with opacity effects. Episodes of enhanced radio luminosity also seem to be related to changes in the pc-scale radio structure where new components are ejected with apparent superluminal velocity (e.g. Wagner et al. 1995; Jorstad et al. 2001).

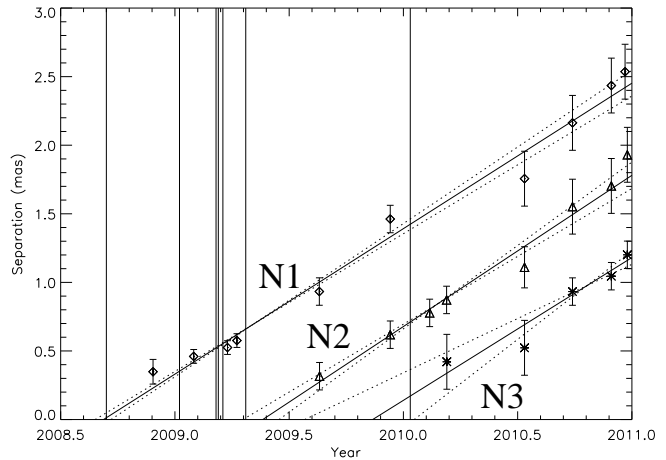


Figure 8. Changes in separation with time between components C and N1, N2, and N3. The solid line represents the regression fit to the data, while the dashed-lines represent the uncertainties from the fit parameters. Error bars are determined as in Section 3.3. Vertical lines show γ -ray flares (Pucella et al. 2008; D’Ammando et al. 2009a; Ciprini & Corbel 2009; D’Ammando et al. 2009b; Pucella et al. 2009; Vercellone et al. 2009; Cutini & Hays 2009; Striani et al. 2010).

Table 3. Proper motion of the jet components of PKS 1510-089. Column 1: source component; Col. 2: number of fitted epochs; Col. 3: apparent speed; Col. 4: zero-separation time; Col. 5: zero-separation time in Julian Date (JD); Col. 6: Reference: 1: this paper; 2: Homan et al. (2001); 3: Lister et al. (2009b); 4: Abdo et al. (2010b); 5: Marscher et al. (2010).

Comp	N_{ep}	β_{app}	T_0	T_0 (JD)	Ref.
J	8	16.2 ± 0.7	1997.42 ± 0.12	2450602 ± 45	1
A	11	15.0 ± 0.7	1994.92 ± 0.18	2449689 ± 66	1,2,3
B	19	18.6 ± 0.5	2005.42 ± 0.11	2453524 ± 40	1,3
N1	10	17.3 ± 0.9	2008.61 ± 0.11	2454689 ± 36	1,4,5
N2	8	18.0 ± 1.9	2009.38 ± 0.17	2454971 ± 62	1,5
N3	5	17.0 ± 4.0	2009.93 ± 0.25	2455171 ± 91	1
C	10	20.2 ± 1.2	1997.85 ± 0.20	2450759 ± 73	3
D	8	18.9 ± 1.3	1999.10 ± 0.25	2451215 ± 91	3
E	7	14.8 ± 0.9	2000.20 ± 0.20	2451617 ± 73	3
F	6	19.1 ± 1.5	2004.42 ± 0.28	2453129 ± 73	3

In the following we discuss our results on the multi-epoch analysis of the total intensity and polarimetric radio properties, and we compare the source activity at various frequency ranges.

4.1 Superluminal motion and polarization analysis

By means of the multi-epoch analysis of the parsec-scale structure of PKS 1510-089, various knots emerging from the core at different times have been detected. In particular, we obtain a solid estimate for one of the components detected

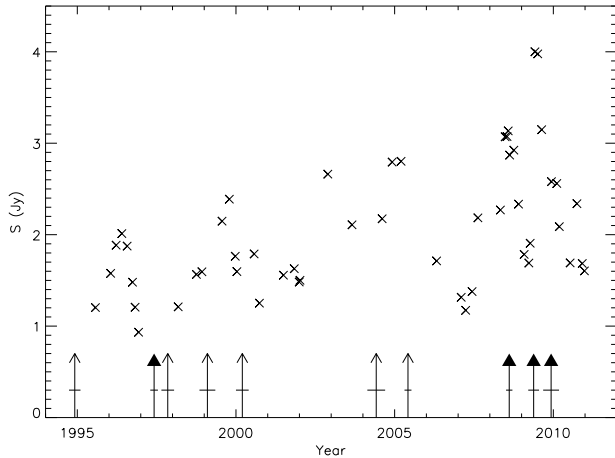


Figure 9. The 15-GHz lightcurve from VLBA MOJAVE data. The uncertainties on the flux density are within the symbols. Thin arrows represent the fitted ejection date of superluminal components from Lister et al. (2009b), while thick arrows refer to the jet components studied in this paper. Each arrow refers to a different superluminal component. The horizontal bars indicate the uncertainty on the ejection date.

between 1999 and 2001, thanks to the addition of 5 new position measurements at 4.8 and 8.4 GHz. Interestingly, comparing the properties of the knots analysed in this paper with those studied in previous works (Table 3) we found that all the knots are separating from the core with an apparent velocity that ranges between $15c$ and $20c$, and all the jet components are well aligned along the same position angle, suggesting that no jet precession is taking place on a time lag longer than a decade in our frame.

In Fig. 9, we report the time of zero separation of all the components ejected between 1994 and 2010, either analysed in this paper, or from the literature. The ejection of a new component likely occurs roughly once per year. The gaps between 2000 and 2004 is likely due to sparse observations available, precluding to reliably follow the evolution of the source components in this period.

Since 1995, in addition to the typical variability interchanging low-activity with high-activity states, the source shows on average a slight increase of the total flux density (Fig. 9). However, the sparse distribution of the data points does not allow us to unambiguously relate the ejection date of the superluminal components, represented by the arrows in Fig. 9, with the various states of the source variability.

From the analysis of the parsec-scale resolution data we could construct the lightcurves for the core and jet components separately, and to study a connection between the total intensity and the polarized emission. The core has high degree of variability, both in the total intensity flux density and in polarization properties, but the data points are too sparse to compare changes in the total intensity and polarized emission throughout the entire time interval. An interesting case is represented by the simultaneous enhancement of the total intensity flux density and the decrease of the fractional polarization observed in the second half of 1999, and the rotation of EVPA around May-July 2001, with a swing of 85° and 130° at 8.4 and 15 GHz respectively (Fig. 6). Possible explanations may be

related either to variation in the opacity in a newly ejected self-absorbed component, or to a highly ordered magnetic field produced by the compression of tangled magnetic fields by shocks. In the former scenario the evolution of the jet knot implies a change between the opacity regimes. As a consequence both the total intensity and the polarized flux densities should decrease during the transition, whereas the magnetic field should jump by 90 degrees. As the opacity decreases, the total flux density should increase in the optically-thick part of the spectrum, while the polarization percentage decreases. As the emitting region expands becoming optically-thin, the radio emission decreases, while the fractional polarization increases and the magnetic field flips of 90 degrees, going back to its original value. It must be noted that changes of the EVPA of 90° are expected from opacity effects during the transition between the two regimes. Since the process is quite fast, a dense time sampling of the polarization information (as the one obtained between 2007 and 2010, Fig. 10) is crucial to detect the transition between the regimes. A sparser sampling, like the one between 1999 and 2001 (Fig. 6), may provide EVPA changes larger/smaller than the expected 90° . The transition between the optically-thick and -thin regimes occurs in the presence of high opacity values (e.g. $\tau \sim 5 - 10$, see for example Aller (1970) and Pacholczyk (1970) for a detailed discussion). Such opacity would cause a dramatic drop of the total intensity flux density during the transition. The lack of observations during the first half of 1999, i.e. when the new jet component should have originated, do not allow us to unambiguously confirm the opacity scenario. However, the increase of the total flux density observed between 1999 and 2000 is difficult to explain in the presence of such high values of the opacity, making this scenario unlikely.

The alternative scenario assumes the formation of a shock that causes the compression of the plasma along the propagation axis. This generates the amplification of the perpendicular component of the magnetic field with respect to the parallel one, and an enhancement of the luminosity. This scenario would predict an increase of the fractional polarization instead of the drop observed close to the radio outburst. However, we must note that if the shock is oblique instead of transverse, the expected variations in the polarization properties are different, and strongly related to the obliqueness of the shock itself, and to the characteristics of the underlying magnetic field like its order and strength. Therefore, a reliable interpretation of the observed polarization trends requires a much better sampling than that available between 1998-2001 (Fig. 6), leaving the debate on the nature of the main mechanism at work still open.

The analysis of the lightcurves and polarization trends between 1998 and 2001, shown in Fig. 6, suggests that the variations of the total intensity flux density and the polarization properties may be explained by both the previous scenarios. Indeed, the total intensity and polarization properties can be related to the evolution (likely adiabatic expansion) of either a new jet component or a shock originated at the beginning of 1999. Support to this interpretation comes from the detection of a superluminal component that possibly originated in 1999.10 ± 0.25 (Lister et al. 2009b). The rotation of the angle found in

2001 may be explained considering that this new component moves far enough from the core to be resolved and the intrinsic polarized emission of the core can be separated from that of the jet.

4.2 Multifrequency analysis

The lightcurves considered in the above explanation would require a more frequent sampling and for this reason a definitive interpretation of the physical mechanisms at work is precluded. A similar consideration may apply to explain the source behaviour around April 2009, when information at other wavelengths (e.g. Abdo et al. 2010b; Marscher et al. 2010) is available. The multiwavelength lightcurve presented by Abdo et al. (2010b) shows a flux density enhancement around that period that is first detected at 230 GHz, and after some delay at lower frequencies. The same behaviour is visible in Fig. 11 where the lightcurves at 15 and 43 GHz³ have been compared. From Fig. 11 we see that the flux densities at both frequencies have a similar behaviour, where the 43-GHz data points seem to anticipate those at lower frequency. Interestingly, just after March 2009, when several γ -ray flares have been detected (D’Ammando et al. 2011), the flux density at 43 GHz becomes higher than that at 15 GHz implying a change in the opacity of the component. The maximum of the radio emission is then reached in April 2009 when another strong γ -ray flare was detected (Cutini & Hays 2009). In correspondence of this luminosity enhancement the polarization percentage drops while the EVPA changes by about 75° (Fig. 10) at both 15 and 43 GHz becoming parallel to the jet direction. In the same period a strong rotation of the optical polarization vector (Marscher et al. 2010) has been detected together with the ejection of a new superluminal component observed at 15 GHz (Fig. 8), and already reported by Abdo et al. (2010b), and at 43 GHz (Marscher et al. 2010). A similar example of dramatic rotation of the polarization angle and a drop of the fractional polarization in coincidence with a γ -ray flare was found in the blazar 3C 279, indicating a co-spatiality of the optical and γ -ray emission region (Abdo et al. 2010c). This has been explained assuming a non-axisymmetric structure of the emitting region, likely a curved jet trajectory, rather than a perpendicular shock moving in an axially symmetric jet as we suggested in Section 4.1. In this case, the degree and angle of polarization strictly depends on the instantaneous angle formed by the direction of the motion with our line of sight (Abdo et al. 2010c). The similarity between 3C 279 and PKS 1510-089 suggests a common origin also for the emission at high energy and in the radio band, and the time lag in the flux density behaviour may be due to opacity effects as the shock passes by. A co-spatiality of the γ -ray and radio emitting region was also claimed for the BL Lac object OJ 287, where two γ -ray flaring episodes occurred close in time with two major millimeter outbursts (Agudo et al. 2011).

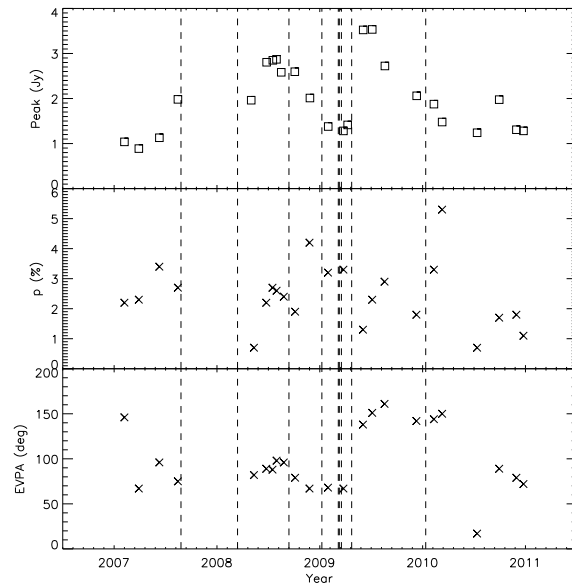


Figure 10. Multi-epoch 15-GHz VLBA peak flux density, restored with the same beam size (*upper panel*), fractional polarization (*middle panel*), and polarization angle (*lower panel*) of the core component of PKS 1510-089. Uncertainties are within the symbols. Vertical lines are relative to high-state γ -ray activity (Pucella et al. 2008; D’Ammando et al. 2009a; Ciprini & Corbel 2009; D’Ammando et al. 2009b; Pucella et al. 2009; Vercellone et al. 2009; Cutini & Hays 2009; Striani et al. 2010).

In PKS 1510-089, the variation in the polarization angle at both 15 and 43 GHz suggests a change in the magnetic field orientation in the compact component rather than Faraday effects caused by an external screen. Changes in the polarization angle of the same magnitude at different wavelengths were reported by Homan et al. (2002b) who monitored the behaviour of a sample of 12 blazars by means of dual-frequency VLBA observations.

It is worth noting that, as in the case of 3C 279 where no changes in the radio band could be found related to the γ -ray flare (Abdo et al. 2010c), in PKS 1510-089 no obvious connection between the γ -ray activity detected in March 2009 (D’Ammando et al. 2011) and the radio flux density behaviour has been found, suggesting that during this flare the synchrotron radiation in the radio band is not yet fully optically thin.

5 CONCLUSIONS

We have presented results from the analysis of multi-epoch polarimetric VLBI, Space-VLBI and archival VLBA data from the MOJAVE programme of the flat spectrum radio quasar PKS 1510-089 spanning over 15 years (1995-2010). This source shows a pc-scale core-jet structure where superluminal knots are ejected at different times. From the multi-epoch observations we found that the emission of new blobs is roughly constant with a time lag of about one year. Furthermore, the various jet components are moving away from the core with an apparent superluminal speed in the range between 15c and 20c and roughly with the same

³ All the values at 43 GHz presented in this paper are from the Large VLBA Project: Total & Polarized Intensity Images of Gamma-Ray Bright Blazars at 43 GHz, and available at http://www.bu.edu/blazars/VLBA_GLAST/1510.html.

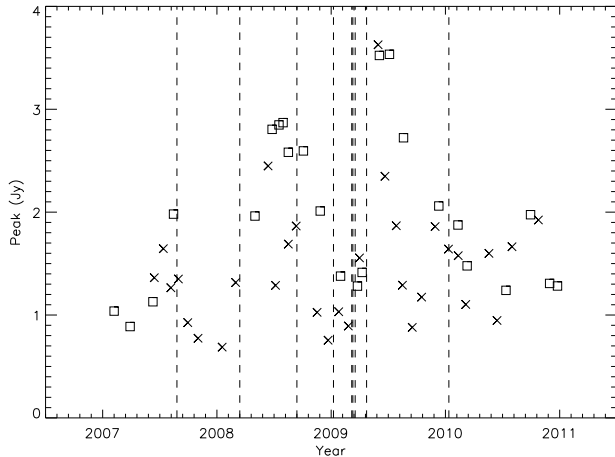


Figure 11. Multi-epoch peak flux density at 15 GHz (squares) and 43 GHz (crosses) of the central component of PKS 1510-089. Vertical lines are relative to high-state γ -ray activity (Pucella et al. 2008; D’Ammando et al. 2009a; Ciprini & Corbel 2009; D’Ammando et al. 2009b; Pucella et al. 2009; Vercellone et al. 2009; Cutini & Hays 2009; Striani et al. 2010).

position angle, suggesting that the precession of the jet is not relevant on the timescale of decades in our frame. Both the total intensity and the polarized flux density of the core component show high level of variability. Our analysis shows that occasionally the EVPA has abrupt changes of about 90 degrees becoming roughly perpendicular to the jet direction during episodes related to enhanced radio emission and opacity variations. These properties may be explained assuming a change between the optically-thick and optically-thin regime as a consequence of a shock that varies the opacity. In this context, the luminosity locally increases due to the compression of the plasma in the direction of the shock propagation, causing the amplification of the perpendicular component of the magnetic field with respect to the parallel one, and the EVPA becomes parallel to the direction of the shock propagation. The observed properties may also be explained as due to a highly ordered magnetic field produced by either an oblique shock or a transverse one propagating down a jet with a curved trajectory. In this case the angle of the electric vector and level of polarization strictly depend on the instantaneous angle formed by the direction of the shock with our line of sight, thus explaining changes in the polarization angle different from the 90 degrees expected during the transition between the opacity regimes. However, the aforementioned scenarios cannot describe the source behaviour after all the detected flares and more monitoring multiwavelength campaigns are needed to properly understand the physical processes occurring in this source.

ACKNOWLEDGMENTS

We thank the anonymous referee for reading the manuscript carefully and making valuable suggestions. The authors are

grateful to G. Brunetti for fruitful discussion. This research has made use of data from the MOJAVE database that is maintained by the MOJAVE team (Lister et al., 2009, AJ, 137, 3718). The VLBA and VLA are operated by the US National Radio Astronomy Observatory which is a facility of the National Science Foundation operated under cooperative agreement by Associated Universities, Inc. This research has made use of the NASA/IPAC Extragalactic Database NED which is operated by the JPL, Californian Institute of Technology, under contract with the National Aeronautics and Space Administration.

APPENDIX A: MOJAVE MULTI-EPOCH MONITORING (1995-2010)

To better characterize the evolution of the source structure with a unique approach we re-analysed VLBA data at 15 GHz from the MOJAVE programme already published by Lister et al. (2009b) and Homan et al. (2001). Data from each epoch were modelfitted as described in Section 3.3, providing a homogeneous set of observations with the same data analysis procedure.

The identification and monitoring of the source components is critical when two subsequent epochs are separated by a long time interval. Indeed, if the observation time coverage is sparse, it becomes very difficult to identify the same component at the various epochs. By comparing the multi-epoch visibility data we found that the source components could be reliably followed only in the observations from 1995 July to 1998 December, and since 2007.

Between 1995 and 1998 we could identify and follow a jet knot for which we derive an angular separation rate of 0.918 ± 0.041 mas/yr, corresponding to an apparent separation velocity $\beta_{\text{app}} = 15.0 \pm 0.7$. For this component Homan et al. (2001) derived an apparent speed of 15.7 ± 0.4 if converted in the cosmology used in this paper. From the linear back-extrapolation fit (Fig. A1) we estimate that the jet component was originated in 1994.92 ± 0.18 .

Between 2007 and 2010, the pc-scale radio morphology displayed a core-jet structure with the presence of four knots, three of which have been discussed in Section 3.3. The other knot we found increases its separation to the core with a rate of 1.134 ± 0.035 , corresponding to an apparent velocity $\beta_{\text{app}} = 18.6 \pm 0.5$, and it should have been originated in 2005.42 ± 0.11 (Fig. A2). For this component Lister et al. (2009b) derived a separation speed of 17.0 ± 2.6 , and the ejection date 2005.87 ± 0.25 . The kinematic properties of the jet components are reported in Table 3.

Between 1999 and 2006 the observations are too sparse in time to allow a reliable identification of the same source component throughout the various data sets.

REFERENCES

- Abdo, A.A., Ackermann, M., Ajello, M., et al. 2010a, ApJ, 715, 429
- Abdo, A.A., Ackermann, M., Agudo, I., et al. 2010b, ApJ, 721, 1425

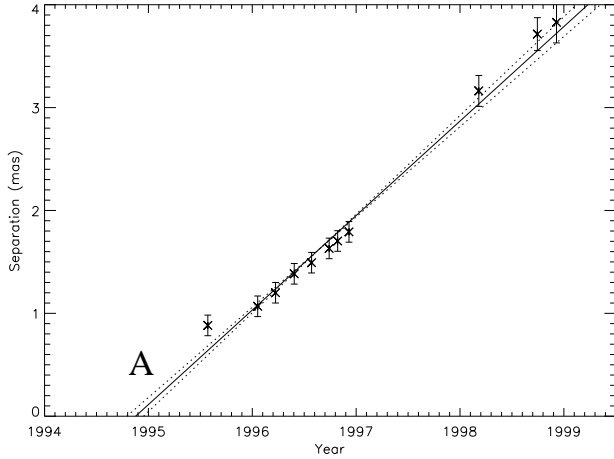


Figure A1. Changes in separation with time between the core and the jet component A. The solid line represents the regression fit to the data, while the dashed-lines represent the uncertainties from the fit parameters. Error bars are determined as in Section 3.3.

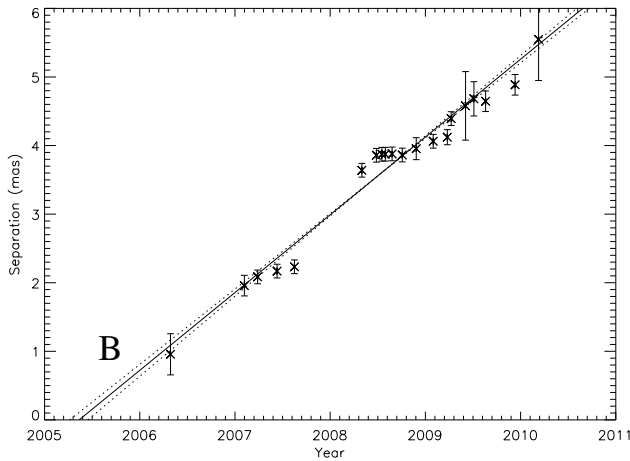


Figure A2. Changes in separation with time between the core and the jet component B. The solid line represents the regression fit to the data, while the dashed-lines represent the uncertainties from the fit parameters. Error bars are determined as in Section 3.3.

Abdo, A.A., Ackermann, M., Ajello, M., et al. 2010c, *Nature*, 463, 919
 Agudo, I., Jorstad, S.G., Marscher, A.P., et al. 2011, *ApJ*, 726, 13
 Aller, H.D. 1970, *ApJ*, 161, 19
 Ciprini, S., Corbel, S. 2009, *ATel*, 1897
 Conway, J.E., Pearson, T.J., Readhead, A.C.S., et al. 1992, *ApJ*, 396, 62
 Cutini, S., Hays, E. 2009, *ATel*, 2033
 D'Ammando F., Bulgarelli, A., Vercellone, S., et al. 2008, *ATel*, 1436
 D'Ammando, F., Vercellone, S., Tavani, M. et al. 2009a, *ATel*, 1957
 D'Ammando, F., Pucella, G., Raitieri, C.M., et al. 2009b, *A&A*, 508, 181

D'Ammando, F., Raitieri, C.M., Villata, M., et al. 2011, *A&A*, 529, 145
 Homan, D.C., Ojha, R., Wardle, J.F.C., Roberts, D.H., Aller, M.F., Aller, H.D., Hughes, P.A. 2001, *ApJ*, 549, 840
 Homan, D.C., Wardle, J.F.C., Cheung, C.C., Roberts, D.H., Attridge, J.M. 2002a, *ApJ*, 580, 742
 Homan, D.C., Ojha, R., Wardle, J.F.C., Roberts, D.H., Aller, M.F., Aller, H.D., Hughes, P.A. 2002b, *ApJ*, 568, 99
 Hughes, P.A., Aller, H.D., Aller, M.F. 1992, *ApJ*, 396, 469
 Jorstad, S.G., Marscher, A.P., Mattox, J.R., et al. 2001, *ApJS*, 134, 181
 Jorstad, S.G., Marscher, A.P., Lister, M.L., et al. 2005, *AJ*, 130, 1418
 Lähteenmäki, A., Valtaoja, E. 2003, *ApJ*, 590, 95
 Lister, M.L., Tingay, S.J., Preston, R.A. 2001, *ApJ*, 554, 964
 Lister, M.L., Homan, D.C., Kadler, M., Kellermann, K.I., Kovalev, Y.Y., Ros, E., Savolainen, T., Zensus, J.A. 2009a, *ApJ*, 696, 22
 Lister, M.L., Cohen, M.H., Homan, D.C., et al. 2009b, *AJ*, 138, 1874
 Lister, M.L., Aller, H.D., Aller, M.F., et al., 2009c, *AJ*, 137, 3718
 Marscher, A.P., Gear, W.K. 1985, *ApJ*, 298, 114
 Marscher, A.P., Jorstad, S.G., Larionov, V.M., et al. 2010, *ApJL*, 710, 126
 Pacholczyk, A.G. 1970, *Radio Astrophysics*, Freeman and Co., San Francisco
 Pearson, T.J., Readhead, A.C.S. 1988, *ApJ*, 328, 114
 Polatidis, A.G., Conway, J.E. 2003, *PASA*, 20, 69
 Pucella, G., Vittorini, V., D'Ammando, F., et al. 2008, *A&A*, 491, 21
 Pucella, G., D'Ammando, F., Tavani, M., et al. 2009, *ATel*, 1968
 Pushkarev, A.B., Kovalev, Y.Y., Lister, M.L., Savolainen, T. 2009, *A&A*, 507, 33
 Pushkarev, A.B., Kovalev, Y.Y., Lister, M.L. 2010, *ApJ*, 722, 7
 Savolainen, T., Homan, D.C., Hovatta, T., Kadler, M., Kovalev, Y.Y., Lister, M.L., Ros, E., Zensus, J.A. 2010, *A&A*, 512, 24
 Simard-Normandin, M., Kronberg, P.P., Button, S. 1984, *ApJS*, 45, 97
 Striani, E., Verrecchia, F., Tavani, M., et al. 2010, *ATel*, 2385
 Thompson, D.J., Djorgovski, S., de Carvalho, R. 1990, *PASP*, 102, 1235
 Tramacere, A. 2008, *ATel*, 1743
 Venturi, T., Dallacasa, D., Orfei, A., et al. 2001, *A&A*, 379, 755
 Vercellone, S., D'Ammando, F., Pucella, G., et al. 2009, *ATel*, 1976
 Wagner, S.J., Camenzind, M., Dreissigacker, O., et al. 1995, *A&A*, 298, 688